Evolution of Single Crystalline Dendrites from Nanoparticles through Oriented Attachment

Yao Cheng,[†,‡] Yuansheng Wang,*[,†] Daqin Chen,[†] and Feng Bao[†]

Fujian Institute of Research on the Structure of Matter, Chinese Academy of Sciences, Fuzhou, Fujian 350002, China, and Graduate School of the Chinese Academy of Sciences, Beijing 100039, China

Received: September 3, 2004; In Final Form: November 4, 2004

Single crystalline $PbMoO_4$ dendrites were prepared by a simple hydrothermal method in the presence of surfactants. The formation and evolution of these dendrites was investigated by transmission electron microscopy, and the results clearly showed that the dendritic structure was achieved through oriented attachment of nanoparticles along crystallographically specific direction while the traditional Ostwald ripening mechanism also acted to form the initial particles before attachment and smooth the morphology of the dendrites after attachment.

Introduction

There is increasing attention on the morphology and size control of material synthesized on the micro- and nanoscale since the discovery of carbon nanotube (CNT) by Iijima[1] due to the fact that morphology and size play very important roles in determining the optic, magnetic, and electric properties of materials. Traditional solution processes, especially the hydrothermal methods, have been widely used for synthesizing various nanomaterials. Among the crystal growth mechanisms in solution system, the well-known Ostwald ripening, in which the growth of crystals has typically been thought to occur by atom-by-atom addition to an inorganic or organic template or by dissolution of unstable phases and reprecipitation of the more stable phase,[2] is generally believed to be the main one. Recently, to explain the mechanisms by which dislocations form during early growth of crystals, Lee and Banfield presented a new crystal growth mechanism involving attachment between two or more nanoparticles followed by sharing a common crystallographic orientation and joining at the planar interfaces.[3] Alivisatos highlighted this growth mechanism termed as "oriented attachment" and predicted that oriented attachment may enable the preparation of interesting artificial materials,[4] and then an increasing number of reports about nanocrystal growth relevant to such mechanism are followed. With the help of kinetic modeling and high-resolution transmission electron microscopy (HRTEM) observation, Huang et al. illustrated that early crystal growth of both H_2O-ZnS and mercaptoethanol-capped ZnS during hydrothermal process occurs predominantly via oriented attachment.[5] Pacholski et al. reported the formation of high-quality single crystalline ZnO nanorods based on oriented attachment of quasi-spherical nanoparticles.[6] Liu et al. found the nanorod-directed epitaxial aggregation of $ZnWO_4$ in solution system.[7]

Recently, novel hierarchical self-assembly structures constructed by nanorods or nanowires have attracted considerable attention. Comblike structures consisting of periodic arrays of single crystalline ZnO nanowires were synthesized by Yan et al. in vapor transport and condensation systems;[8] $BaWO_4$ fishbone-like nanostructures made of nanorods were achieved in cationic water/oil microemulsion system by Xu et al.;[9] Dendritic and flower-shaped PbS nanocrystals have also been prepared by hydrothermal and microwave-heating method,[10−12] respectively. The exact mechanism for the formation of such hierarchical structure is still unknown, although there have been many discussions about the various factors affecting the structure. Very recently, increasing interests have been focused on the formation mechanism of hierarchical structures: branched and hyperbranched nanowires were synthesized via a multistep nanocluster-catalyzed vapor−liquid−solid mechanism;[13,14] surfactant-assisted solution growth and evolution mechanism of dendritic nanostructures with temperature-dependent morphology was discussed.[15,16] It is believed that the oriented attachment along crystallographically specific direction, different from the mostly appeared random aggregation, would offer an additional tool and open a new access to design and synthesis of a single crystal with complex hierarchical structure in which the branching sites could be added as individual nanoparticles. Such complex three-dimensional crystals based on oriented attachment, however, have seldom been reported yet.

Lead molybdate ($PbMoO_4$) with scheelite structure is one of the most important materials in the acousto-optic applications due to its low sound-wave wastage and excellent acousto-optic quality factor.[17] Moreover, lead molybdate was also a promising candidate as a scintillator for the double β decay experiment at temperatures below 100 K.[18] The growth and properties of single crystalline lead molybdate have been reported previously by many authors.[19−22] Herein we present the research results on the formation and evolution mechanism of nanoscaled single crystalline lead molybdate dendrites through hydrothermal process.

Experimental Section

For hydrothermal reactions, all the reagents were of analytical grade and used as received. In a typical synthesis procedure, 0.1 g of MoO_3 was added to the 10 mL of 0.125 M NaOH solution followed by 10 min of vigorous agitation to form a homogeneous Na_2MoO_4 solution, and then 2 mL of poly-

* Corresponding author. Tel: +86-591-8370-5402. Fax: +86-591-8370-5402. E-mail: yswang@fjirsm.ac.cn.

† Fujian Institute of Research on the Structure of Matter, Chinese Academy of Sciences.

‡ Graduate School of the Chinese Academy of Sciences.

10.1021/jp0460240 CCC: $30.25 © 2005 American Chemical Society
Published on Web 12/24/2004

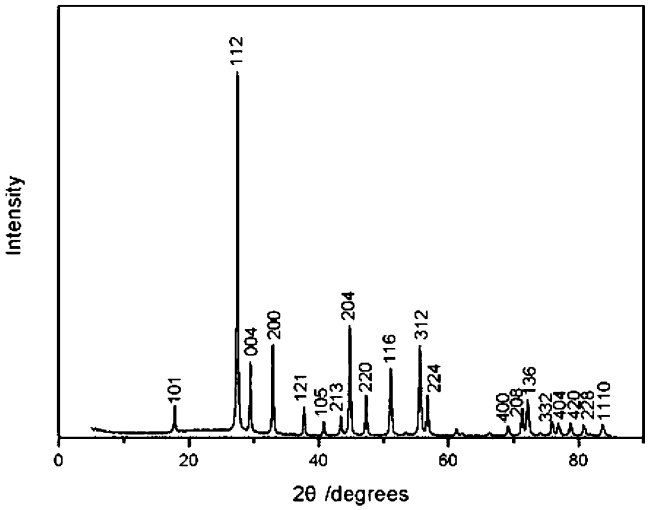

Figure 1. XRD pattern of the as-synthesized $PbMoO_4$ sample after 20 h reaction.

(ethylene glycol) 400 (PEG-400) and 0.25 g of $Pb(CH_3COO)_2 \cdot 3H_2O$ were added into the above aqueous solution. The mixture was transferred into a Teflon-lined stainless steel autoclave of 20 mL capacity. The sealed tank was heated to and maintained at 160 °C for 20 h in an oven, then was taken out and cooled-down to room temperature under ambiance condition. The resulting gray-white precipitates were collected by filtration and washed with deionized water and pure ethanol respectively for several times, then dried in air. For further study on the crystal formation and evolution process, some more experiments were also performed for different reaction time with other conditions unchanged.

To identify the product structure, powder X-ray diffraction (XRD) patterns of the samples were recorded by RIGAKU-DMAX2500 X-ray diffractometer with Cu $K\alpha$ radiation (λ = 1.54056 Å) at a scanning rate of 5°/min for 2θ ranging from 5° to 85°. The morphologies and microstructures of the as-synthesized samples were observed by XL30 ESEM-TMP scanning electron microscope (SEM) at 25 kV and JEOL-2010 transmission electron microscope (TEM) at 200 kV, respectively. Two-dimensional Fourier transform patterns of high-resolution TEM (HRTEM) images and the reconstructed lattice images from them were used to characterize the lattice defects and the coalescence behavior of the nanoparticles.

Results and Discussion

The XRD pattern of the as-synthesized sample aged at 160 °C for 20 h shown in Figure 1 confirms the scheelite structure of the entire dendrites. All the diffraction peaks can be indexed by a body-centered tetragonal phase of scheelite structure with lattice constants a = 5.433 Å and c =12.11 Å, which is in agreement with the literature value (JCPDS No. 77-0431). The strong and sharp peaks indicate the high crystallinity of $PbMoO_4$.

The SEM images shown in Figure 2 clearly reveal the three-dimensional dendritic structure of $PbMoO_4$ crystallites. The low magnification image (Figure 2A) indicates the high yield of such dendrites. The higher magnification image (Figure 2B) demonstrates a typical dendrite resembling morphologically the human backbone, in which four branches perpendicular to the stem are evenly spaced alternately on the major stem with a regular periodicity of about 100 nm. Each branch has a cuspate end like a sword. In general, the length of the stem and the diameter of the branch range from 1 to 10 μm and 60 to 150 nm, respectively.

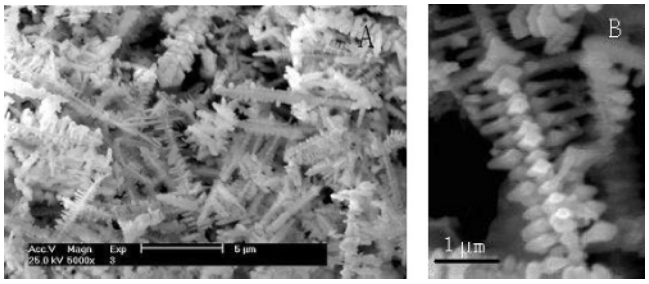

Figure 2. SEM images of $PbMoO_4$ dendritic crystallites prepared by hydrothermal reaction for 20 h, (A) the low magnification image and (B) the higher magnification image of a single $PbMoO_4$ dendrite.

For a series of samples prepared by hydrothermal reaction with different time, the formation and evolution of dendrites could be monitored by TEM and HRTEM. Figure 3 shows the typical TEM images of $PbMoO_4$ particles hydrothermally reacted at 160 °C for 10 min, 30 min, and 10 h, respectively. After 10 min reaction, many particles with diameter ranging from 30 to 60 nm formed, and some of them attached together as shown in Figure 3A,B. The HRTEM image (Figure 3C) taken from the connecting region of the adjacent particles in Figure 3B shows well-developed (200) lattice planes evidenced by the Fourier transform pattern (upper inset in Figure 3C), indicating the (200) being the bonding plane and thus the epitaxial coalescence of the two particles being along the [100] direction. The reconstructed lattice image (lower inset in Figure 3C) from the specified square area shows clearly the existence of an edge dislocation at the connecting region. The formation of dislocation at the bonding interface is often considered to be a direct consequence of oriented attachment of particles due to small misorientation or atomic nonflatness in the interface, and so marks the occurrence of the initial particle−particle bonding.[3] After reaction time prolonged to 30 min, many 3-armed and 4-armed crystals were found, as shown in Figure 3D,E. The proportion for 3-armed and 4-armed crystals in the sample is about 10% and 50%, respectively. These crystals are believed to be the results of further development of oriented attachment evidenced by the discriminable bottlenecks between the connecting particles. The selected area electron diffraction (SAED) pattern (upper inset in Figure 3F) from the 4-armed particle in Figure 3E can be indexed to the $PbMoO_4$ single crystal along the [001] zone axis, indicating the four arms extending along the ⟨100⟩ directions, respectively. Figure 3F is the HRTEM image taken from a bottleneck region (marked with a square) of the 4-armed particle in Figure 3E, from which the epitaxial (200) contact lattice planes going straight through the connecting region can be recognized. Again, an edge dislocation lined out in the reconstructed lattice image (lower inset in Figure 3F) is found within the connecting region.

After formation of 4-armed structure has been achieved, the main framework of the dendritic crystal has been built. The further oriented attachment would go on to construct more complex dendritic structure by the following two manners. For the first one, new nanoparticle connects to the 4-armed particle at the end of an arm to elongate its length, as manifested in Figure 3G. The Fourier transform analysis based on the HRTEM image of the connecting region confirms the bonding plane and elongating direction being (200) and [100], respectively, as shown in Figure 3H. The corresponding reconstructed lattice image (Figure 3I) from the specified square region indicates the creation of a few edge dislocations during the attachment process. For the second one, a new nanoparticle connects to the 4-armed crystal at the lateral of an arm to form a branch, as

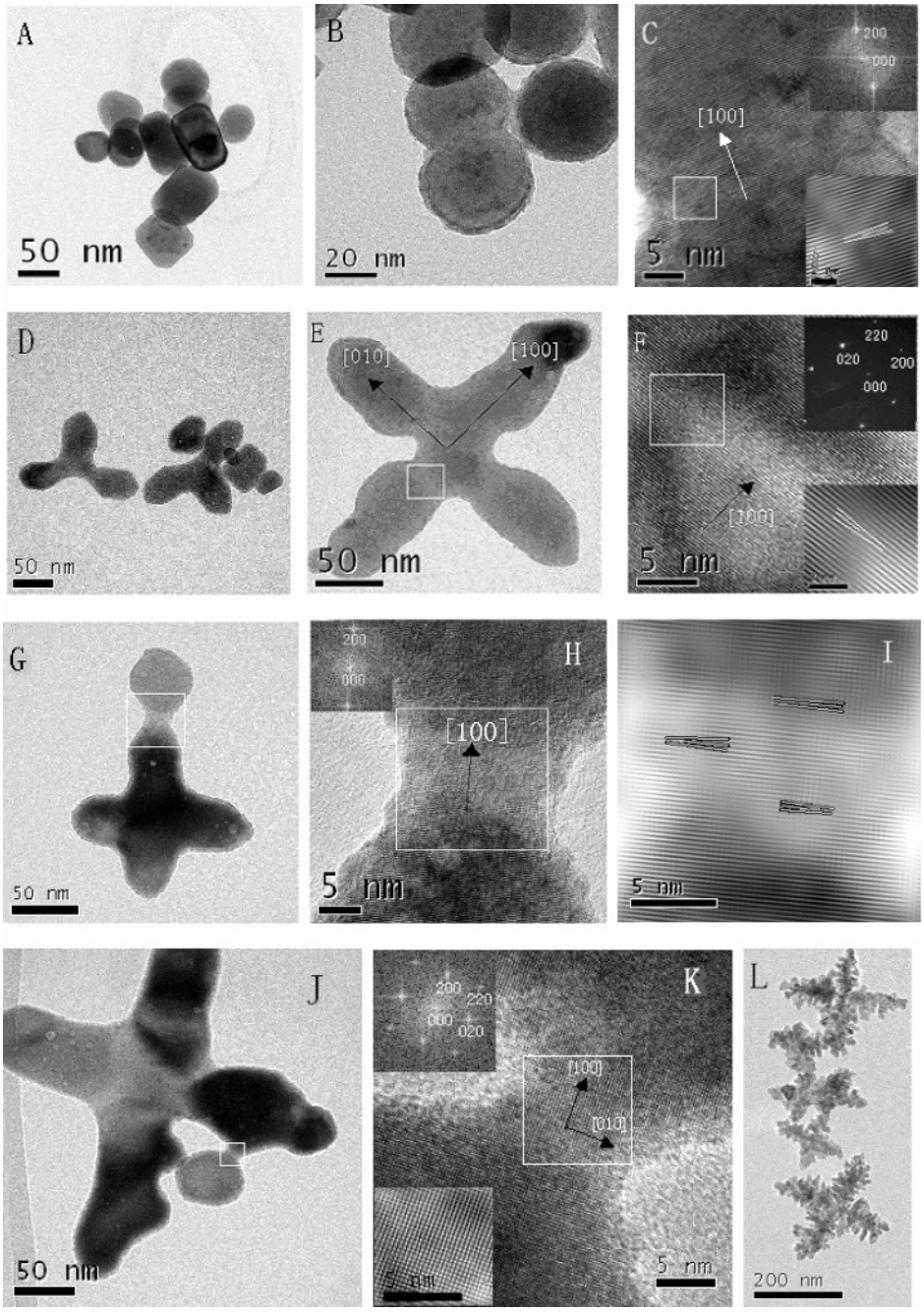

Figure 3. TEM and HRTEM images and SAED patterns of $PbMoO_4$ crystals obtained at the different stages of hydrothermal reaction: (A) the initial particles before attachment; (B) a pair of the typical attached particles; (C) HRTEM image of the connecting region of the attached particles in Figure 3B, the upper inset is the Fourier transform and the lower inset the reconstructed lattice image from the specified square area; (D) the typical 3-armed particles; (E) a typical 4-armed particle; (F) HRTEM image of the connecting region of the attached particles in Figure 3E, the upper inset is the SAED pattern of the 4-armed particle and the lower inset the reconstructed lattice image from the specified square area; (G) TEM image showing attachment of a new particle to elongate the arm; (H) HRTEM image of the bottleneck region in Figure 3G and the corresponding Fourier transform (upper inset); (I) reconstructed image from the square area in Figure 3H; (J) TEM image of attachment of a new particle to the lateral of an arm forming the branch; (K) HRTEM image of the bonding region in Figure 3J, the upper inset is the Fourier transform and the lower inset the reconstructed image from the square region; (L) TEM image of scabbled dendrites.

manifested in Figure 3J. Further analysis aimed at the connecting region (Figure 3K) reaches the same conclusion of epitaxial coalescence as mentioned above. The reconstructed two-dimensional lattice image (lower inset in Figure 3K) from the specified square region in the center of the same figure, however, clearly shows the lattice planes being almost perfectly aligned without any dislocation, revealing that oriented attachment can also produce perfect bonding plane. After hydrothermal reaction duration increased to 10 h, a large amount of scabbled dendrites (about 80% of the whole sample) developed from the previous 4-armed crystals were found, as shown in Figure 3L. The enlarged image of a growing dendrite is shown in Figure 4A, from which it is obvious that many branches are produced through attachment of particles to the stem. The SAED pattern (inset in Figure 4A) also confirms preferential growth of stem along [100] and [010] directions. It is noteworthy that besides those branches lying parallel to the (001) plane, comparatively fewer branches along [001] are also developed and visible as black contrast on the stem. These attachments along [001] taking place at the later stage of dendrite formation change the dendritic

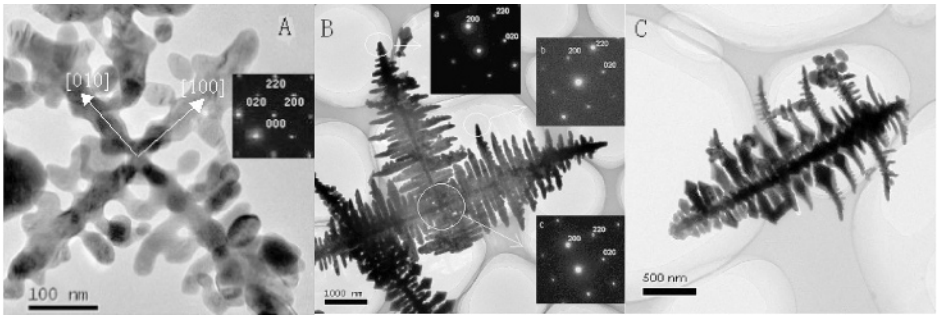

Figure 4. TEM images of the dendrites: (A) a growing dendrite and the corresponding SAED pattern (inset); (B) a grown-up dendrite after 20 h reaction and the corresponding SAED patterns (insets) from the different circled regions; (C) a typical broken dendrite.

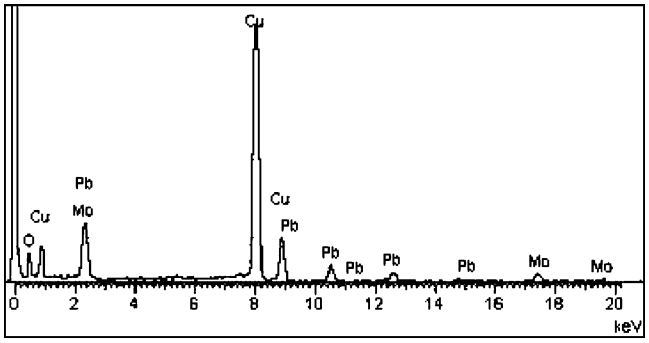

Figure 5. EDX spectrum of the dendrite. The signals of Cu come from the copper grid.

structure from two-dimensional to three-dimensional. Another 10 more hours' reaction enables the further construction of beautiful dendrites, as shown in Figure 4B. The insets in this figure are SAED patterns taken from the stem, the branch, and the central part of the cruciform dendrite. All these SAED patterns are identical and can be indexed to the $PbMoO_4$ phase along the [001] zone axis, indicating the single crystalline nature of the entire dendrite and the preferential growth direction of stems along ⟨100⟩. Being different from the $PbWO_4$ dendrites synthesized by Liu et al.[15] where the crystal shows three crossed stems, the grown-up $PbMoO_4$ has two stems along *a* and *b* axis directions and only short branches along the *c* axis direction. To determine the elemental composition of the dendrite, energy-dispersive X-ray spectroscopy (EDX) was applied. A typical EDX spectrum from the dendrite as shown in Figure 5 confirms that the crystals are composed of only Mo, O, and Pb, and the atomic ratio for Mo:Pb:O is near 1:1:4, in agreement with the expected stoichiometry of the $PbMoO_4$ phase. The absence of Na and C signals in EDX spectrum indicates the effective eliminating of Na and surfactants from the final products through multistep wash. The ideal grown-up crystals should exhibit a symmetrical cruciform dendritic structure. Similar to the SEM result shown in Figure 2, however, most of the grown-up dendrites found by TEM are broken ones such as that shown in Figure 4C. Hereby we suggest that cracking at the central part of the dendrite should be a frequent incident at a later stage of the hydrothermal process due to vigorous movement and impingement of the dendrites in a high-temperature and high-pressure environment, which leads to the large amount of broken dendrites.

Oriented aggregation has been regarded as one of the important crystal growth mechanisms, both in aqueous and nonaqueous solutions. Bonding between the particles reduces overall energy by removing surface energy associated with unsatisfied bonds. Before the bonding of colliding particles, there will be a rotation between the particles driven by Brownian motion and the short-range interactions between the particles to find the low-energy configuration represented by a coherent particle−particle interface, followed by particles sharing a common crystallographic orientation and joining with each other. However, when surfaces are not atomically flat, coherence will then be achieved by lattice distortion in some areas of the interface, which causes the dislocation. The growth of $PbMoO_4$ three-dimensional dendrites through oriented attachment of nanoparticles preferentially along specified crystallographic directions is an interesting phenomenon. Although the exact reason accounting for the specified planes being the preferential connecting planes is not clear, the surfactant PEG-400 may play a key role in such a process because there is no dendrite (only irregular shaped particles instead) found when the reaction is carried out without PEG-400 or in the presence of other surfactant (e.g., PEG-5000 or CTAB) instead of PEG-400. We suggest that the adherence of PEG-400 molecules to the crystal planes of $PbMoO_4$ nanoparticles would occur at the early stage of crystal growth, which would certainly inhibit the further growth of nanoparticles. On the crystal planes with low index (e.g., {200} and {002}), however, the interaction between surfactant molecules and nanoparticles should be relatively weak due to the lower charge density of the plane.[16] So the desorption of PEG-400 molecules from these specific planes would be easier as a consequence of violent thermal disturbance and result in the exposure of these low-index surfaces. Thus, as a consequence, these planes would be free for bonding. As for the body-centered tetragonal scheelite structure with cell parameter *c* being much larger than *a* ($a = 5.433$ Å, $c = 12.11$ Å), the charge density of {200} should be much lower than that of {002}, which makes {200} having precedence over {002} to be the most preferential bonding planes. This explains why oriented attachment takes place preferentially along [100] and [010], and only at the later stage of crystal formation that the growth along [001] begins to occur.

It is noteworthy that the initial particles between which oriented attachment occurs have a definite size distribution from 30 to 60 nm, and no particles with size less than 30 nm participating in the attachment have been found. So it is reasonable to suggest that coarsening by conventional Ostwald ripening mechanism of dissolution and growth of monomer would first occur before the starting of oriented attachment. Furthermore, Ostwald ripening also helps during the coalescence of dendrites in which bottlenecks between adjacent particles being filled up and surfaces of dendrites getting smoothened as evidenced by TEM observations. In this sense, Ostwald ripening not only competes with but also assists the oriented attachment to yield final dendrites.

The temperature-dependent morphology evolution of dendritic microcrystal has been reported previously,[15,16] in which tem-

perature determines the final morphology of the product. In our experiments, however, the dendritic morphology seems to be not so sensitive to the temperature. When the reaction temperature was varied from 100 to 180 °C, the final product morphology is always the same if enough reaction time is given. Moreover, when the same hydrothermal method was applied to synthesize $BaMoO_4$, the similar dendritic structure was also obtained. It is reasonable to suggest that this kind of crystal growth mechanism may generally be applied to the hydrothermal synthesis of other inorganic crystals with body-centered tetragonal scheelite structure.

Conclusions

In summary, we have presented the experimental results that the single crystalline $PbMoO_4$ with complex dendritic structure can be achieved through oriented attachment of nanoparticles along crystallographically specific directions. The traditional Ostwald ripening mechanism also acted to form the initial particles before attachment and smooth the dendritic morphology during the course of attachment. The results validate the previous formation hypothesis of complexed three-dimensional crystalline hierarchical structures in which the branching sites could be added as individual nanoparticles. This crystal growth mode may probably be generally applied to the hydrothermal synthesis of other inorganic crystals with body-centered tetragonal scheelite structure, and furthermore, provide an important approach to the fabrication of specific nanostructured material with improved performances.

Acknowledgment. The research was financially supported by Fujian Provincial Natural Science Foundation, China (Project No. A0320001). We are grateful for the helpful comments from the referees.

References and Notes

(1) Iijima, S. *Nature* **1991**, *354*, 56.
(2) Banfield, J. F.; Welch, S. A.; Zhang, H.; Ebert, T. T.; Penn, R. L. *Science* **2000**, *289*, 751.
(3) Penn, R. L.; Banfield, J. F. *Science* **1998**, *281*, 969.
(4) Alivisatos, A. P. *Science* **2000**, *289*, 736.
(5) Huang, F.; Zhang, H.; Banfield, J. F. *J. Phys. Chem. B* **2003**, *107*, 10470.
(6) Pacholski, C.; Kornowski, A.; Weller, H. *Angew. Chem., Int. Ed.* **2002**, *41*, 1188.
(7) Liu, B.; Yu, S.; Li, L.; Zhang, F.; Zhang, Q.; Yoshimura, M.; Shen, P. *J. Phys. Chem. B* **2004**, *108*, 2788.
(8) Yan, H.; He, R.; Johnson, J.; Law, M.; Saykally, R. J.; Yang, P. *J. Am. Chem. Soc.* **2003**, *125*, 4728.
(9) Zhang, X.; Xie, Y.; Xu, F.; Tian, X. *J. Colloid Interface Sci.* **2004**, *274*, 118.
(10) Wang, D.; Yu, D.; Shao, M.; Liu, X.; Yu, W.; Qian, Y. *J. Cryst. Growth* **2003**, *257*, 384.
(11) Ni, Y.; Liu, H.; Wang, F.; Liang, Y.; Hong, J.; Ma, X.; Xu, Z. *Cryst. Growth Des.* **2004**, *4* (4), 759.
(12) Kuang, D.; Xa, A.; Fang, Y.; Liu, H.; Frommen, C.; Fenske, D. *Adv. Mater.* **2003**, *15*, 1747.
(13) Dick, K. A.; Deppert, K.; Larsson, M. W.; Martensson, T.; Seifert, W.; Wallenberg, L. R.; Samuelson, L. *Nature Mater.* **2004**, *3*, 380.
(14) Wang, D.; Qian, F.; Yang, C.; Zhong, Z.; Lieber, C. M. *Nano Lett.* **2004**, *4* (5), 871.
(15) Liu, B.; Yu, S.; Li, L.; Zhang, Q.; Zhang, F.; Jiang, K. *Angew. Chem. Int. Ed.* **2004**, *43*, 4745.
(16) Huang, Q.; Gao, L. *Chem. Lett.* **2004**, *33* (10), 1338.
(17) Senguttuvan, N.; Babu, S. M.; Subramanian, C. *Mater. Sci. Eng.* **1997**, *B47*, 269.
(18) Minowa, M.; Itakura, K.; Motiyama, S.; Ootani, W. *Nucl. Instrum. Methods A* **1992**, *320*, 500.
(19) Zhang, Y.; Holzwarth, N. A. W.; Williams, R. T. *Phys. Rev. B* **1998**, *57* (20), 12738.
(20) Brown, S.; Marshall, A.; Hirst, P. *Mater. Sci Eng. A* **1993**, *173*, 23.
(21) Gabrielian, V. T.; Fedorova, L. M.; Tkachenko, E. B.; Neiman, A. Y.; Nikogosian, N. S. *Cryst. Res. Technol.* **1986**, *21*, 439.
(22) Vesselinov, I. *J. Cryst. Growth* **1996**, *167*, 725.